PNAS RESEARCH ARTICLE | ECOLOGY OPEN ACCESS

Spreading processes with mutations over multilayer networks

Mansi Sood[a], Anirudh Sridhar[b], Rashad Eletreby[c], Chai Wah Wu[d], Simon A. Levin[e], Osman Yağan[a,f,1], and H. Vincent Poor[b,1]

Contributed by H. Vincent Poor; received February 8, 2023; accepted April 22, 2023; reviewed by Alex Arenas and Jeffrey Shaman

A key scientific challenge during the outbreak of novel infectious diseases is to predict how the course of the epidemic changes under countermeasures that limit interaction in the population. Most epidemiological models do not consider the role of mutations and heterogeneity in the type of contact events. However, pathogens have the capacity to mutate in response to changing environments, especially caused by the increase in population immunity to existing strains, and the emergence of new pathogen strains poses a continued threat to public health. Further, in the light of differing transmission risks in different congregate settings (e.g., schools and offices), different mitigation strategies may need to be adopted to control the spread of infection. We analyze a multilayer multistrain model by simultaneously accounting for i) pathways for mutations in the pathogen leading to the emergence of new pathogen strains, and ii) differing transmission risks in different settings, modeled as network layers. Assuming complete cross-immunity among strains, namely, recovery from any infection prevents infection with any other (an assumption that will need to be relaxed to deal with COVID-19 or influenza), we derive the key epidemiological parameters for the multilayer multistrain framework. We demonstrate that reductions to existing models that discount heterogeneity in either the strain or the network layers may lead to incorrect predictions. Our results highlight that the impact of imposing/lifting mitigation measures concerning different contact network layers (e.g., school closures or work-from-home policies) should be evaluated in connection with their effect on the likelihood of the emergence of new strains.

network epidemics | multilayer networks | mutations | agent-based models | branching processes

Significance

In this work, we provide a mathematical framework to analyze spreading processes triggered by mutating contagions in the light of nonpharmaceutical interventions such as lockdowns that reduce physical contact in different social settings (e.g., schools and offices). To this end, we analyze multistrain spreading on multilayer contact networks, where network layers represent different social settings. Our results highlight that imposing/lifting interventions in different network layers should be evaluated in connection with their effect on the emergence of new strains. Moreover, reductions to existing models that do not simultaneously account for heterogeneity in the contagions strains and network layers may lead to incorrect predictions of the likelihood of the emergence of an epidemic outbreak.

The recent outbreak of the COVID-19 pandemic, fueled by the novel coronavirus SARS-CoV-2 led to a devastating loss of human life and upended livelihoods worldwide (1). The highly transmissible, virulent, and rapidly mutating nature of the SARS-CoV-2 coronavirus (2) led to an unprecedented burden on critical healthcare infrastructure. The emergence of new strains of the pathogen as a result of mutations poses a continued risk to public health (3, 4). Moreover, when a new strain is introduced to a host population, pharmaceutical interventions often take time to be developed, tested, and made widely accessible (5, 6). In the absence of widespread access to treatment and vaccines, policymakers are faced with the challenging problem of taming the outbreak with nonpharmaceutical interventions (NPIs) that encourage physical distancing in the host population to suppress the growth rate of new infections (7–9). However, the ensuing socioeconomic burden (10, 11) of NPIs, such as lockdowns, makes it necessary to understand how imposing restrictions in different social settings (e.g., schools, offices, etc.) alter the course of the epidemic outbreak.

Epidemiological models that analyze the speed and scale of the spread of infection can be broadly classified under two approaches. The first approach assumes homogeneous mixing, i.e., the population is well mixed, and an infected individual is equally likely to infect any individual in the population regardless of location and social interactions (12, 13). The second is a network-based approach that explicitly models the contact patterns among individuals in the population and the probability of transmission through any given contact (14–16). Structural properties of the contact network such as heterogeneity in type of contacts (17), clustering (e.g., presence of tightly connected communities) (18), centrality (e.g., presence of superspreaders) (19, 20), and degree-degree correlations (21) are known to have profound implications for disease spread and its control (22, 23). To understand the impact of NPIs that lead to reduction in physical contacts, network-based epidemiological models have been employed widely in the context of infectious diseases, including COVID-19 (24–26).

In addition to the contact structure within the host population, the course of an infectious disease is critically tied to evolutionary adaptations or mutations in the pathogen. There is growing evidence for the zoonotic origin of disease outbreaks, including COVID-19, SARS, and H1N1 influenza, as a result of cross-species transmission

Author contributions: M.S., O.Y., and H.V.P. designed research; M.S., A.S., C.W.W., and O.Y. performed research; M.S., A.S., C.W.W., S.A.L., O.Y., and H.V.P. contributed new reagents/analytic tools; M.S., A.S., R.E., S.A.L., O.Y., and H.V.P. analyzed data; and M.S., A.S., R.E., C.W.W., S.A.L., O.Y., and H.V.P. wrote the paper.

Reviewers: A.A., Rovira i Virgili University; and J.S., Columbia University.

The authors declare no competing interest.

[1]To whom correspondence may be addressed. Email: oyagan@andrew.cmu.edu or poor@princeton.edu.

This article contains supporting information online at http://www.pnas.org/lookup/suppl/doi:10.1073/pnas.2302245120/-/DCSupplemental.

Published June 8, 2023.

and subsequent evolutionary adaptations (27–31). When pathogens enter new species, they are often poorly adapted to the physiological environment in the new hosts and undergo mutations to adapt to the new hosts (27). The resulting variants or strains of the pathogen have varying risks of transmission, commonly measured through the reproduction number or R_0, which quantifies the mean number of secondary infections triggered by an infected individual (32, 33). Moreover, even when a sizeable fraction of the population gains immunity through vaccination or natural infection, the emergence of new variants that can evade the acquired immunity poses a continued threat to public health (3, 4). A growing body of work (27, 34–44) has highlighted the need for developing multistrain epidemiological models that account for evolutionary adaptations in the pathogen. For instance, there is a vast literature on phylodynamics (38–41) which examines how epidemiological and evolutionary processes interact to impact pathogen phylogenies. The past decade has also seen the development of network-based models to identify risk factors for the emergence of pathogens in the light of different contact patterns (27, 34, 42, 43). Further, a recent study (34) demonstrated that models that do not consider evolutionary adaptations may lead to incorrect predictions about spreading processes with mutations.

Most existing network-based approaches that analyze the spread of contagions with mutations center on single-layered contact networks, where transmissibility, i.e., the probability that an infective individual passes on the infection to a contact, depends on the type of strain but not on the nature of link/contact over which the infection is transmitted (27, 34, 43). However, different congregate settings such as schools, hospitals, offices, and private social gatherings pose varied transmission risks (45). Recently, multilayer networks have been used to model human contact networks (24–26, 33, 46), where each layer represents a different social setting in which an individual participates. While multilayer contact networks (20, 47–57) and multistrain contagions(27, 34–37, 43) have been extensively studied in separate contexts, there has been a dearth of analysis on simultaneously accounting for the multistrain network structure and multistrain spreading.

In this paper, we build upon the mathematical theory for the multistrain model proposed in refs. 27 and 34 to account for the multilayer structure typical to human contact networks, where different network layers correspond to different social settings in which individuals congregate. Specifically, we assume that the transmissibility depends not only on the type of strain carried by an infective individual but also on the social setting (modeled through a network layer) in which they meet their contacts. The proposed framework allows us to study how closing/opening different network layers impacts the spreading characteristics of a contagion.

While the bulk of our discussion is on spreading processes with mutations in the context of infectious diseases, our results also hold promise for applications in modeling social contagions, e.g., news items circulating in social networks (34, 58). Similar to different strains of a pathogen arising through mutations, different versions of the information are created as the content is altered on social media platforms (59). The resulting variants of the information may have varying propensities to be circulated in the social network. Moreover, with the burst of social media platforms, potential applications of our multilayer analysis of evolving contagions include analyzing multiplatform spread of misinformation where the information gets altered across different platforms.

Materials and Methods

Contact Network. We consider a population of size n with members in the set $\mathcal{N} = \{1, \ldots, n\}$. Patterns of interaction in the host population are encoded in the contact network where an edge is drawn between two nodes if they can come in contact and potentially transmit the infection. To account for variability in transmission risks associated with different social settings (e.g., neighborhood, school, workplace), we consider a multilayer contact network (47), where each network layer corresponds to a unique social setting. For simplicity, we focus on the case where each individual can participate independently in two network layers denoted by $\mathbb{F}$ and $\mathbb{W}$, respectively. For instance, the network layer $\mathbb{F}$ can be used to model the spread of infection between friends residing in the same neighborhood, while the network layer $\mathbb{W}$ can model the spread of infections among individuals who congregate for work.

In order to model participation in each network layer, we first independently label each node as nonparticipating in network layer a with probability α_a and participating in network layer a with probability $1 - \alpha_a$, where $0 \leq \alpha_a \leq 1$, and where $a \in \{f, w\}$. Next, for each node that participates in network layer a, the number of its neighbors in layer a is drawn from a degree distribution, denoted by $\{\tilde{p}^a_{k'}, k = 0, 1, \ldots, n\}$, where $a \in \{f, w\}$. Under this formulation, the degree of a node in layer a, denoted by $\{p^a_{k'}, k = 0, 1, \ldots\}$, with $a \in \{f, w\}$, is given by

$$p^a_k = (1 - \alpha_a)\tilde{p}^a_k + \alpha_a \mathbf{1}\{k = 0\}, \quad k = 0, 1, \ldots, \qquad [\mathbf{1}]$$

where $\mathbf{1}\{\}$ denotes the indicator random variable, admitting the value one when $k = 0$ and zero when $k \geq 1$. We generate both layers independently according to the configuration model (60, 61) with the degree distribution given through Eq. **1**. For notational simplicity, we say that edges in network $\mathbb{F}$ (respectively, $\mathbb{H}$) are of type f (respectively, type w). The multilayer contact network, denoted as $\mathbb{H}$, is constructed by taking the disjoint union ($\sqcup\!\!\sqcup$) of network layers $\mathbb{W}$ and $\mathbb{F}$ (Fig. 1). We assume that the network $\mathbb{H}$ is static and focus on the emergent spreading behavior in the limit of infinite population size ($n \to \infty$).

Spreading Process. We adopt a multistrain spreading process (27) to the multilayer network setting as follows. For each layer, the evolutionary adaptations in the pathogen are modeled by corresponding mutation matrices. Let m denote the number of pathogen strains coexisting in a population. For network layer $\mathbb{F}$ (respectively, $\mathbb{W}$), the mutation matrix, denoted by $\boldsymbol{\mu}^f$ (respectively, $\boldsymbol{\mu}^w$) is a $m \times m$ matrix. The entry μ^f_{ij} (respectively, μ^w_{ij}) denotes the probability that strain i mutates to strain j within a host who got infected through a type f (respectively, type w) link, with $\sum_j \mu^f_{ij} = 1$ (respectively, $\sum_j \mu^w_{ij} = 1$). Given that an individual carrying strain i makes an infectious contact through a type f (respectively, type w) edge, the newly infected individual acquires strain j with probability μ^f_{ij} (respectively, μ^w_{ij}). For infectious diseases where the epidemiological and evolutionary processes occur at a similar timescale and mutations of the pathogen occur within the host and each new infection offers

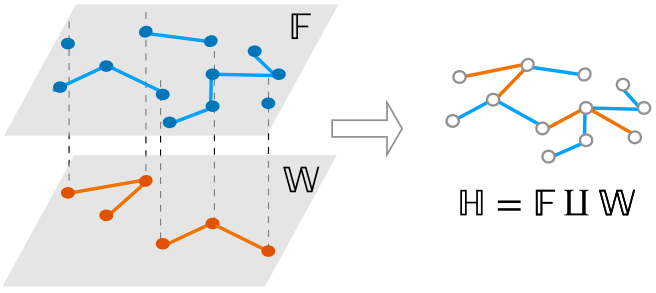

Fig. 1. Multilayer network model: An illustration of a two-layer contact network for modeling the spread of an infection over the friendship/neighborhood network $\mathbb{F}$ and work network $\mathbb{W}$. The resultant contact network $\mathbb{H} = \mathbb{F} \sqcup\!\!\sqcup \mathbb{W}$. Neighboring nodes in $\mathbb{H}$ can transmit infections to their neighbors either through links in the $\mathbb{F}$ network (i.e., through type f links) or $\mathbb{W}$ network (through type w links).

an opportunity for mutation (27), the mutation matrices do not depend on the network structure (27) and $\boldsymbol{\mu}^w = \boldsymbol{\mu}^f$*. In the succeeding discussion, we focus on the setting where two strains of the pathogen are dominant and assume $m = 2$. We denote

$$\boldsymbol{\mu}^f = \begin{bmatrix} \mu^f_{11} & \mu^f_{12} \\ \mu^f_{21} & \mu^f_{22} \end{bmatrix}, \qquad \boldsymbol{\mu}^w = \begin{bmatrix} \mu^w_{11} & \mu^w_{12} \\ \mu^w_{21} & \mu^w_{22} \end{bmatrix}.$$

We consider a SIR spreading process wherein each individual is susceptible (S), meaning that they have not yet been exposed to the contagion; infectious (I), meaning that they have received the contagion and are currently spreading it to their contacts; or recovered (R), meaning that they are no longer spreading the contagion. We first describe how the time scale of interactions are modeled for on a single-layer network (14, 15) with a single strain and later extend it to the multilayer setting. We assume that an infectious individual v_x transmits the infection to a susceptible contact v_y with probability T_{xy}, which is given by

$$T_{xy} = 1 - e^{-r_{xy}\tau_x},$$

where r_{xy} denotes the average rate of being in close-enough contact over the link from v_x to v_y, and τ_x is the time v_x keeps spreading the contagion; i.e., the time it takes for v_x to become recovered.

In a multilayer setting, the spread of a contagion is expected to vary across different layers due to different interaction rates r_{xy}, resulting in different probabilities T_{xy} across the layers. For example, due to different time scales or rates of interactions across layers, two nodes v_x and v_y may have a very different rate of being in close-enough contact in the school layer versus the neighborhood layer. In the context of viral propagation, it would be expected that the recovery time τ_x of individuals is the same across different layers. With this model, we can also see that the emergence of a new strain will affect the transmissibility across a given link between nodes v_x and v_y, potentially by the modification of both the rate of interaction and the recovery time. For example, a new strain may have better spreading capabilities in certain distances between individuals, which may change the rate at which v_x and v_y come into close-enough contact (given that the threshold of being close enough depends on the characteristics of the strain). Similarly, a new strain may cause individuals to have a shorter or longer recovery period.

We let the probability that an infective individual passes on the infection to their neighbor be a function of the type of strain and the type of link over which the infection is transmitted. For each strain i, we let $T^{a,i}_{xy}$ stand for the probability of transmission over a link (between v_x and v_y) in network layer a, where $a \in \{f, w\}$. For simplicity, we assume that the random variables corresponding to the interactions and recovery rates ($r^{a,i}_{xy}$ and $\tau^{a,i}_x$) are independent and identically distributed (i.i.d.) with probability densities $P^{a,i}(r)$ and $P^{a,i}(\tau)$, respectively. Finally, we define T^a_i as the mean probability of transmission of strain i in network layer a, i.e.,

$$T^a_i := < T^{a,i}_{xy} > = 1 - \int_0^\infty \int_0^\infty e^{-r^{a,i}_{xy}\tau^{a,i}_x} P^{a,i}(r^{a,i}_{xy}) P^{a,i}(\tau^{a,i}_x) \mathrm{d}r^{a,i}_{xy} \mathrm{d}\tau^{a,i}_x.$$

We refer to T^a_i as the transmissibility of strain i over network layer a and note that $0 \leq T^a_i \leq 1$. With these definitions, it has been shown in refs. 15 and 14 that, under certain assumptions, the contagion propagates over network layer a as if transmission probabilities across all edges in layer a were equal to the transmissibility of that layer for the purposes of computing the threshold, probability, and expected size of epidemics. In fact, this mean-field approach has been shown in ref. 15 (by proving that the SIR process is isomorphic to bond percolation) to give the same results as the SIR process for the epidemic threshold and the final size of an epidemic in all cases. For the probability of epidemics, it has been shown in ref. 15 that the mean-field approach provides the same results as the SIR process as long as the recovery time of nodes follows a degenerate probability distribution (i.e., as long as the recovery times are deterministic across different nodes).

*In the context of information propagation, different strains (34) may correspond to different versions of the information. Therefore, we let the mutation probabilities depend on the network layer to provide a more general contagion model.

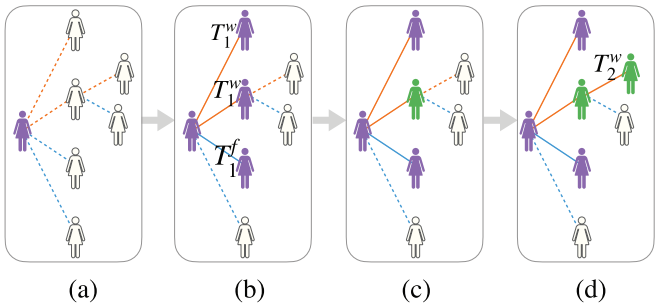

Fig. 2. Multistrain spreading model: An illustration of the multistrain model with 2 strains on a contact network comprising 2 layers—(*A*) An arbitrarily chosen seed node acquires strain 1; (*B*) The seed node independently infects their susceptible neighbors connected through type f (respectively, type w) links with probability T^f_1 (respectively, T^w_1); (*C*) After infection, the pathogen mutates to strain 2 within the hosts with probabilities given by mutation matrices $\boldsymbol{\mu}^f$ and $\boldsymbol{\mu}^w$; (*D*) The infected nodes in turn infect their neighbors with transmission probabilities governed by the strain that they are carrying (i.e., strain 1 or strain 2) and the type of edge used to infect their neighbors (i.e., type 1 or type 2). The process terminates when no further infections are possible.

We define $m \times m$ diagonal matrices $\boldsymbol{T}^f$ (respectively, $\boldsymbol{T}^w$), with $[T^f_i]$ (respectively, $[T^w_i]$) representing the transmissibility of strain i over a type f link (respectively, type w link), for $i = 1, \ldots, m$. For $m = 2$ strains, we have

$$\boldsymbol{T}^f = \begin{bmatrix} T^f_1 & 0 \\ 0 & T^f_2 \end{bmatrix}, \qquad \boldsymbol{T}^w = \begin{bmatrix} T^w_1 & 0 \\ 0 & T^w_2 \end{bmatrix}.$$

We consider the following multistrain spreading process (Fig. 2). The process starts when a randomly chosen seed node is infected with strain 1. We refer to such a seed node as the initial infective and the subsequently infected nodes as later-generation infectives. The seed node independently infects their susceptible neighbors connected through type f (respectively, type w) links with probability T^f_1 (respectively, T^w_1). We assume that coinfection is not possible, and after infection, the pathogen mutates to strain i within the hosts with probabilities given by mutation matrices $\boldsymbol{\mu}^f$ and $\boldsymbol{\mu}^w$. Further, in line with (27, 34), we assume that once an individual becomes recovered after being infected with either strain, then they can not be reinfected with any strain. The infected nodes in turn infect their neighbors independently with transmission probabilities governed by the strain they are carrying (i.e., strain 1 or strain 2) and the type of edge used to infect their neighbors (i.e., type f or type w). The process terminates when no further infections are possible.

We note that this paper is the first effort to develop a framework for the multiscale process discussed. In it, we assume complete cross-immunity between strains: Recovery from any infection prevents infection with any other. This is a good assumption, for example, for myxomatosis but is not a good assumption for influenza or COVID, for which the emergence of new strains is driven by escape from population immunity. The case of incomplete cross-immunity, which is an essential feature of the current pandemic, therefore will be the subject of a follow-up paper. Additional details regarding the Materials and Methods are presented in *SI Appendix*, 1.

Results

Summary of Key Contributions. We provide analytical results for characterizing epidemic outbreaks caused by mutating contagions over multilayer contact networks using tools from multitype branching processes. In particular, we derive three key metrics to characterize the epidemic outbreak. i) The probability of emergence of an epidemic is defined as the probability that a randomly chosen infectious seed node leads to an epidemic, i.e., a positive fraction of nodes get infected in the limit of large network

size. ii) The epidemic threshold defines the critical boundary of the region in the parameter space where a phase transition occurs, leading to the possibility of an epidemic outbreak. Specifically, the epidemic threshold defines a region in the parameter space inside which the outbreak dies out after a finite number of transmissions, while outside that region, the epidemic occurs with a positive probability. iii) Finally, we derive the epidemic size as the conditional mean of the fraction of individuals infected by each type of strain, given that an epidemic outbreak has occurred.

We supplement our theoretical findings with analytical case studies and simulations for different patterns of interaction in the host population and different types of mutation patterns in the pathogens. The multilayer multistrain modeling framework allows for understanding trade-offs, such as the relative impact of countermeasures, including lockdowns that alter the network layers on the emergence of highly contagious strains. For cases where the spread of infection starts with a moderately transmissible strain, we study how imposing/lifting mitigation measures across different layers can alter the course of the epidemic by increasing the risk of mutation to a highly contagious strain. We derive the probability of mutation to a highly transmissible strain which in turn provides a lower bound on the probability of emergence. Through a case study for one-step irreversible mutation patterns, our results highlight that reopening a new layer in the contact network may be considered low-risk based on the transmissibility of the current strain. Still, even a modest increase in infections caused by the additional layer can lead to an epidemic outbreak to be triggered with a much higher probability. Therefore, it is important to evaluate mitigation measures concerning different network layers in connection with their impact on the likelihood of the emergence of new pathogen strains.

Next, we unravel conditions under which we can reduce the multilayer multistrain model to simpler models for accurately characterizing the epidemic outbreak. We show that while a reduction to a single-layer model can accurately predict the epidemic characteristics when the network layers are purely Poisson, a departure from Poisson distribution can lead to incorrect predictions with single-layer models. Moreover, we show that the success of approaches that coalesce the multilayer structure to an equivalent single layer is critically dependent on the dispersion indices of the network layers being perfectly matched. However, in practice, different network layers (representing different congregate settings) are expected to have different structural characteristics, further highlighting the need for considering multilayer network models for predicting the course of an outbreak. Our results further underscore the need for developing epidemiological models that account for heterogeneity among the variants of the contagions as well as the contact network layers.

Probability of Emergence. The first question that we investigate is whether a spreading process started by infecting a randomly chosen seed node with strain 1 causes an outbreak infecting a positive fraction of individuals, i.e., an outbreak of size $\Omega(n)$. Our results are based on multitype branching processes (27, 34, 62, 63). For computing the probability of emergence, we first define probability generating functions (PGFs) of the excess degree distribution. Let $\boldsymbol{d} = (d^f, d^w)$ denote the joint degree over layer f and layer w. We define $g(z^f, z^w)$ as the PGF for joint degree distribution $p_{\boldsymbol{d}} = p^f_{d^f} \cdot p^w_{d^w}$ of a randomly selected seed node, where the parameters z^f (respectively, z^w) correspond to its degree d^f (respectively, d^w) in layer f (respectively, layer w):

$$g(z^f, z^w) = \sum_{\boldsymbol{d}} p_{\boldsymbol{d}} \left(z^f\right)^{d^f} (z^w)^{d^w}. \quad [2]$$

For $a \in \{f, w\}$, we define, $G^a(z^f, z^w)$ as the PGF for excess joint degree distribution for the number of type f and type w contacts of a node reached by following a randomly selected type a edge (later-generation infective/ intermediate host). While computing $G^a(z^f, z^w)$, we discount the type a edge that was used to infect the given node. We have

$$G^f(z^f, z^w) = \sum_{\boldsymbol{d}} \frac{d^f p_{\boldsymbol{d}}}{\langle d^f \rangle} \left(z^f\right)^{d^f - 1} (z^w)^{d^w}, \quad [3]$$

$$G^w(z^f, z^w) = \sum_{\boldsymbol{d}} \frac{d^w p_{\boldsymbol{d}}}{\langle d^w \rangle} \left(z^f\right)^{d^f} (z^w)^{d^w - 1}. \quad [4]$$

The factor $d^f p_{\boldsymbol{d}}/\langle d^f \rangle$ (respectively, $d^w p_{\boldsymbol{d}}/\langle d^w \rangle$) gives the normalized probability that an edge of type f (respectively, type w) is attached (at the other end) to a vertex with colored degree $\boldsymbol{d} = (d^f, d^w)$ (14). Suppose, an arbitrary node u carries strain 1 and transmits the infection to one of its susceptible neighbors, denoted as node v. Since there are two types of links/edges in the contact network and two types of strains circulating in the host population, there are four types of events that lead to the transmission of infection from node u to v, namely, whether edge (u, v) is

(i) type f and no mutation occurs in host v;
(ii) type f and mutation to strain 2 occurs in host v;
(iii) type w and no mutation occurs in host v;
(iv) type w and mutation to strain 2 occurs in host v.

In cases (i) and (iii), there is no mutation in the host node v, and v infects their neighbors in layer f (respectively, layer w) with T_1^f (respectively, T_1^w). In cases (ii) and (iv), strain 1 mutates to strain 2, and v infects its neighbors in layers f and w with transmissibility T_2^f and T_2^w, respectively. For applying a branching process argument (14, 64) and writing recursive equations using PGFs, it is crucial to keep track of both the types of edges used to transmit the infection and the types of strain acquired after mutation. Therefore, we keep a record of the number of newly infected individuals who acquire strain 1 or strain 2 and the type of edge through which they acquired the infection. We define the joint PGFs for transmitted infections over four random variables corresponding to the four infection events (i) to (iv) as follows:

$$\gamma_1(z_1^f, z_2^f, z_1^w, z_2^w) = g\left(1 - T_1^f + T_1^f \left(\sum_{j=1}^{2} \mu_{1j}^f z_j^f\right), 1 - T_1^w + T_1^w \left(\sum_{j=1}^{2} \mu_{1j}^w z_j^w\right)\right).$$

For $a \in \{f, w\}$ and $i \in \{1, 2\}$, denote

$$\Gamma_i^a(z_1^f, z_2^f, z_1^w, z_2^w) = G^a\left(1 - T_i^f + T_i^f \left(\sum_{j=1}^{2} \mu_{ij}^f z_j^f\right), 1 - T_i^w + T_i^w \left(\sum_{j=1}^{2} \mu_{ij}^w z_j^w\right)\right).$$

We show that the quantity $\gamma_1(z_1^f, z_2^f, z_1^w, z_2^w)$ represents the PGF for the number of infection events of each type induced among the neighbors of a seed node when the seed node is infected with

strain 1; *SI Appendix*, 1.A. Furthermore, for $a \in \{f, w\}$ and $i \in \{1, 2\}$, we show that $\Gamma_i^a(z_1^f, z_2^f, z_1^w, z_2^w)$ is the PGF for the number of infection events of each type caused by a later-generation infective (i.e., a typical intermediate host in the process) that received the infection through a type a edge and carries strain i. Our first main result characterizes the probability of emergence when the outbreak starts at an arbitrary node infected with strain 1.

Theorem 1 (Probability of Emergence). *It holds that*

$$\mathbb{P}[Emergence] = 1 - \gamma_1(q_1^f, q_2^f, q_1^w, q_2^w), \quad [5]$$

where, $\left(q_1^f, q_2^f, q_1^w, q_2^w\right)$ *are the smallest nonnegative roots of the fixed point equations:*

$$q_1^f = \Gamma_1^f(q_1^f, q_2^f, q_1^w, q_2^w) \quad [6]$$

$$q_2^f = \Gamma_2^f(q_1^f, q_2^f, q_1^w, q_2^w) \quad [7]$$

$$q_1^w = \Gamma_1^w(q_1^f, q_2^f, q_1^w, q_2^w) \quad [8]$$

$$q_2^w = \Gamma_2^w(q_1^f, q_2^f, q_1^w, q_2^w). \quad [9]$$

Here, for $a \in \{w, f\}$ and $i \in \{1, 2\}$, the term q_i^a can be interpreted as the probability of extinction starting from one later-generation infective carrying strain i (after mutation) which was infected through a type a edge; see *SI Appendix*, 1.A for a detailed proof. Therefore, the probability of emergence of an epidemic is given by the probability that at least one of the infected neighbors of the seed triggers an unbounded chain of transmission events. We note that Theorem 1 provides a strict generalization for the probability of emergence of multistrain spreading on a single layer (27), and we can recover the probability of emergence for the case of single layer by substituting $\boldsymbol{T}^f = \boldsymbol{T}^w$ and $\boldsymbol{\mu}^f = \boldsymbol{\mu}^w$ in Eqs. **6**– **9**.

Epidemic Threshold. Next, we characterize the epidemic threshold, which is commonly studied as a metric to characterize an epidemic and ascertain risk factors (65). Let λ_f and λ_w denote the first moments of the distributions $\{p_{df}^f\}$ and $\{p_{dw}^w\}$, respectively. Let $\langle d_f^2 \rangle$ and $\langle d_w^2 \rangle$ denote the corresponding second moments for distributions $\{p_{df}^f\}$ and $\{p_{dw}^w\}$. Further, define β_f and β_w as the mean of the excess degree distributions respectively in the two layers. We have

$$\beta_f := \frac{\langle d_f^2 \rangle - \lambda_f}{\lambda_f} \quad \text{and} \quad \beta_w := \frac{\langle d_w^2 \rangle - \lambda_w}{\lambda_w}. \quad [10]$$

Theorem 2 (Epidemic Threshold). *For*

$$\boldsymbol{J} = \begin{bmatrix} T_1^f \mu_{11}^f \beta_f & T_1^f \mu_{12}^f \beta_f & T_1^w \mu_{11}^w \lambda_w & T_1^w \mu_{12}^w \lambda_w \\ T_2^f \mu_{21}^f \beta_f & T_2^f \mu_{22}^f \beta_f & T_2^w \mu_{21}^w \lambda_w & T_2^w \mu_{22}^w \lambda_w \\ T_1^f \mu_{11}^f \lambda_f & T_1^f \mu_{12}^f \lambda_f & T_1^w \mu_{11}^w \beta_w & T_1^w \mu_{12}^w \beta_w \\ T_2^f \mu_{21}^f \lambda_f & T_2^f \mu_{22}^f \lambda_f & T_2^w \mu_{21}^w \beta_w & T_2^w \mu_{22}^w \beta_w \end{bmatrix}, \quad [11]$$

let $\rho(\boldsymbol{J})$ *denote the spectral radius of* $\boldsymbol{J}$*. The epidemic threshold is given by* $\rho(\boldsymbol{J}) = 1$.

The above theorem states that the epidemic threshold is tied to the spectral radius of the Jacobian matrix J, i.e., if $\rho(\boldsymbol{J}) > 1$, then an epidemic occurs with a positive probability, whereas if $\rho(\boldsymbol{J}) \leq 1$, then with high probability, the infection causes a self-limited outbreak, where the fraction of infected nodes vanishes to 0 as $n \to \infty$. The matrix $\boldsymbol{J}$ is obtained while determining the stability of the fixed point of the recursive equations in Theorem 1 by linearization around $q_1^f = q_2^f = q_1^w = q_2^w = 1$ (*SI Appendix*, 1.B). We note that when the mutation matrix is indecomposable, meaning that each type of strain eventually may lead to the emergence of any other type of strain with a positive probability, the threshold theorem for multitype branching processes (27) guarantees if $\rho(\boldsymbol{J}) \leq 1$, then $q_i^a = 1$, whereas if $\rho(\boldsymbol{J}) > 1$, then $0 \leq q_i^a < 1$, where $i \in \{1, 2\}$ and $a \in \{f, w\}$. For decomposable processes, the threshold theorem (27) guarantees extinction ($q_i^a = 1$) if $\rho(\boldsymbol{J}) \leq 1$; however, the uniqueness of the fixed-point solution does not necessarily hold when $\rho(\boldsymbol{J}) > 1$.

Our next result reveals the interplay of the network structure and the transmission parameters in determining the threshold for emergence of an epidemic outbreak.

Lemma 1. *When* $T_1^w/T_1^f = T_2^w/T_2^f = c$*, where* $c > 0$*, and let* $\boldsymbol{\mu} = \boldsymbol{\mu}^f = \boldsymbol{\mu}^w$*, we get,*

$$\rho(\boldsymbol{J}) = \rho\left(\begin{bmatrix} \beta_f & c\lambda_w \\ \lambda_f & c\beta_w \end{bmatrix}\right) \times \rho(\boldsymbol{T}^f \boldsymbol{\mu}). \quad [12]$$

Lemma 1 follows from the observation that with $T_1^w/T_1^f = T_2^w/T_2^f = c$, we can express $\boldsymbol{J}$ as a Kronecker product of two matrices (denoted by $\otimes$), as below.

$$\boldsymbol{J} = \begin{bmatrix} T_1^f \mu_{11} \beta_f & T_1^f \mu_{12} \beta_f & T_1^w \mu_{11} \lambda_w & T_1^w \mu_{12} \lambda_w \\ T_2^f \mu_{21} \beta_f & T_2^f \mu_{22} \beta_f & T_2^w \mu_{21} \lambda_w & T_2^w \mu_{22} \lambda_w \\ T_1^f \mu_{11} \lambda_f & T_1^f \mu_{12} \lambda_f & T_1^w \mu_{11} \beta_w & T_1^w \mu_{12} \beta_w \\ T_2^f \mu_{21} \lambda_f & T_2^f \mu_{22} \lambda_f & T_2^w \mu_{21} \beta_w & T_2^w \mu_{22} \beta_w \end{bmatrix} = \begin{bmatrix} \beta_f & c\lambda_w \\ \lambda_f & c\beta_w \end{bmatrix} \otimes (\boldsymbol{T}^f \boldsymbol{\mu}).$$

The first assumption $T_1^w/T_2^w = T_1^f/T_2^f$ is consistent with scenarios where the ratio of the transmissibility of the two strains in each layer is a property of the contagion, not the contact networks. This is supported by the assumption (26) that interventions such as social distancing measures reduce the transmissibility of the disease by a specific coefficient for the entire network layer. The second assumption ($\boldsymbol{\mu}^f = \boldsymbol{\mu}^w$) in Lemma 1 is motivated by the occurrence of mutations within individual hosts (27).

Lastly, we observe that Lemma 1 provides a unified analysis for the epidemic threshold for the case with a single strain or a single layer (27, 47). To obtain the epidemic threshold for multistrain spreading on a single-layer network, we first obtain the spectral radius of $\boldsymbol{J}$, denoted by $\rho^{\text{MS-SL}}$. Next, invoking Eq. **12** with $T_i^f = T_i^w$ and setting the mean degree of one of the layers as zero gives $\rho^{\text{MS-SL}}$. For instance, we can set $\lambda_w = \beta_w = 0$, yielding

$$\rho^{\text{MS-SL}} = \beta_f \times \rho(\boldsymbol{T}^f \boldsymbol{\mu}), \quad [13]$$

where β_f corresponds to the mean of the excess degree distribution for the contact network with a single layer f. For single

strain spreading on a multilayer contact network, we substitute $T_1^f = T_2^f$ in Eq. **12**, which gives $\rho(\boldsymbol{T^f}\boldsymbol{\mu}) = T^f\rho(\boldsymbol{\mu}) = T^f$, yielding the corresponding spectral radius, denoted as $\rho^{\text{SS-ML}}$,

$$\rho^{\text{SS-ML}} = \rho\left(\begin{bmatrix}\beta_f & c\lambda_w\\ \lambda_f & c\beta_w\end{bmatrix}\right) \times T^f. \qquad [14]$$

The corresponding epidemic thresholds are obtained by setting the above spectral radii $\rho^{\text{MS-SL}}$ and $\rho^{\text{SS-ML}}$ to one.

Mean Epidemic Size. Next, we compute the mean epidemic size and the mean fraction of nodes infected by each strain. Knowing the fraction of individuals infected by each strain is vital for cases when different pathogen strains have different transmissibility and virulence. In such cases, predicting the expected fraction of the population hit by the more severe strain can help scale healthcare resources in time.

For computing the mean epidemic size, we consider the zero-temperature random-field Ising model on Bethe lattices (66), as done in ref. 34. We refer to a node as being active if it is infected with either of the two strains (strain 1 or strain 2), and inactive otherwise. Since $\mathbb{H}$ is locally tree-like (67), we consider the following hierarchical structure, such that at the top level, there is a single node (the *root*). The probability that an arbitrarily chosen root node is infected with strain 1 (respectively, strain 2), gives the mean fraction of individuals infected by strain 1 (respectively, strain 2). Let Q_1 (respectively, Q_2) denote the probability that the root node is active and carries strain 1 (respectively, strain 2). We label the levels of the tree from level $\ell = 0$ at the bottom to level $\ell = \infty$ at the top, i.e., the root. We assume that coinfection is not possible. Specifically, if a node receives x_1^f (respectively, x_1^w) infections of strain 1 through type f (respectively, type w) links and x_2^f (respectively, x_2^w) infections of strain 2 through type f (respectively, type w) links, then after mutation, it becomes infected by strain i with probability

$$\frac{\mu_{1i}^f x_1^f + \mu_{2i}^f x_2^f + \mu_{1i}^w x_1^w + \mu_{2i}^w x_2^w}{x_1^f + x_2^f + x_1^w + x_2^w},$$

where $i \in \{1, 2\}$. For $a \in \{f, w\}$, and $i \in \{1, 2\}$, let $q_{\ell+1,i}^a$ denote the probability that a node at level $\ell + 1$ is active, carries strain i, and is connected to a node at level $\ell + 2$ through a type a edge. Our next result characterizes the mean fraction of individuals infected by each type of strain during an epidemic outbreak. As a crucial step toward deriving the mean fraction of infected individuals, we first show that for $i = 1, 2$, we have

$$q_{\ell+1,i}^f = \sum_{\boldsymbol{d}} \frac{d^f p_{\boldsymbol{d}}}{\langle d^f\rangle} f_i(q_{\ell,1}^f, q_{\ell,2}^f, q_{\ell,1}^w, q_{\ell,2}^w, d^f - 1, d^w), \qquad [15]$$

$$q_{\ell+1,i}^w = \sum_{\boldsymbol{d}} \frac{d^w p_{\boldsymbol{d}}}{\langle d^w\rangle} f_i(q_{\ell,1}^f, q_{\ell,2}^f, q_{\ell,1}^w, q_{\ell,2}^w, d^f, d^w - 1)., \qquad [16]$$

We let $q_{\infty,i}^a$ denote the limit of $q_{\ell,i}^a$ as $\ell \to \infty$.

Theorem 3 (Epidemic Size). *For $i = 1, 2$, we have*

$$Q_i = \sum_{\boldsymbol{d}} p_{\boldsymbol{d}} f_i(q_{\infty,1}^f, q_{\infty,2}^f, q_{\infty,1}^w, q_{\infty,2}^w, d^f, d^w), \qquad [17]$$

with the mean epidemic size

$$Q = Q_1 + Q_2,$$

where $f_i(u_1^f, u_2^f, u_1^w, u_2^w, z^f, z^w)$ is given in SI Appendix, 1.C.

Here, $f_i(u_1^f, u_2^f, u_1^w, u_2^w, z^f, z^w)$ denotes the probability that an arbitrary node u at level $\ell + 1$ gets infected with strain 1 through neighbors in level ℓ such that there are z^f and z^w neighbors of node u in layers f and w, respectively. A precise definition of $f_i(u_1^f, u_2^f, u_1^w, u_2^w, z^f, z^w)$ and a proof of Theorem 3 is presented in *SI Appendix*, 1.C.

Experimental Evaluation. In this section, we present numerical studies on different contact structures and transmission patterns. We focus on the setting where the fitness landscape consists of two types of strains and two types of network layers. The two network layers are independently generated using the configuration model after sampling degree sequences from the distributions $\{p_k^f,\ k = 0, 1, \ldots\}$ and $\{p_k^w,\ k = 0, 1, \ldots\}$. We first investigate the case when the network layers follow a Poisson degree distribution. Additionally, we consider the power-law degree distribution (*SI Appendix*, 1.D), which is widely used (68) in modeling the structure of several real-world networks, including social networks. Further, to account for mitigation measures that limit the number of people who can congregate in the different layers, we let the degree distributions for the two layers follow the power law degree distribution with an exponential cutoff; *SI Appendix*, 1.D.

The spreading process starts when a randomly chosen node is selected as the seed carrying strain 1 (Fig. 2). In subsequent time steps, each node independently infects their neighbors with a transmission probability that depends on both the type of strain carried and the nature of link through which contact occurs. After infection, the pathogen mutates within the hosts with probabilities given by the mutation matrices. In cases where a susceptible node comes in contact with multiple infectious neighbors, we resolve exposure to multiple infections as follows. If a node receives x_1^f (respectively, x_1^w) infections of strain 1 through type f (respectively, type w) links, and x_2^f (respectively, x_2^w) infections of strain 2 through type f (respectively, type w) links, with probability $\frac{\mu_{1i}^f x_1^f + \mu_{2i}^f x_2^f + \mu_{1i}^w x_1^w + \mu_{2i}^w x_2^w}{x_1^f + x_2^f + x_1^w + x_2^w}$, after mutation, it is infected with strain i, which it spreads to its neighbors in layer a with probability T_i^a, where $i \in \{1, 2\}$ and $a \in \{f, w\}$. The process reaches a steady state and terminates when no new infections are possible. Throughout, we let Q denote the mean epidemic size and Q_1 and Q_2, respectively, denote the final fraction of individuals infected by each strain in the steady state.

Next, we compare our analytical results for the probability of emergence and expected epidemic size (Theorems 1–3) with empirical values obtained by simulating the spread of infection over multiple independent experiments. We consider a contact network where the degree distribution for each layer is Poisson with parameters λ_f and λ_w, respectively. To model scenarios where there is a risk of the emergence of a new, more transmissible strain (strain 2) starting from strain 1, we set $T_1^f = 0.6$, $T_2^f = 0.8$, $T_1^w = 0.7$, $T_2^w = 0.9$, $\mu_{11}^f = \mu_{11}^w = 0.1$, and $\mu_{22}^f = \mu_{22}^w = 0.95$, and we fix the number of nodes n = 10,000. We plot the probability of emergence and epidemic size in Fig. 3. We indicate the epidemic threshold as the vertical dashed line where we observe a phase transition, with the probability and expected epidemic size sharply increasing from zero to one as the epidemic threshold is exceeded. We plot the expected fraction of individuals infected by each strain (Q_1 and Q_2). The total epidemic size Q is the sum of the fraction of individuals infected by each strain ($Q = Q_1 + Q_2$). In Fig. 4, we consider

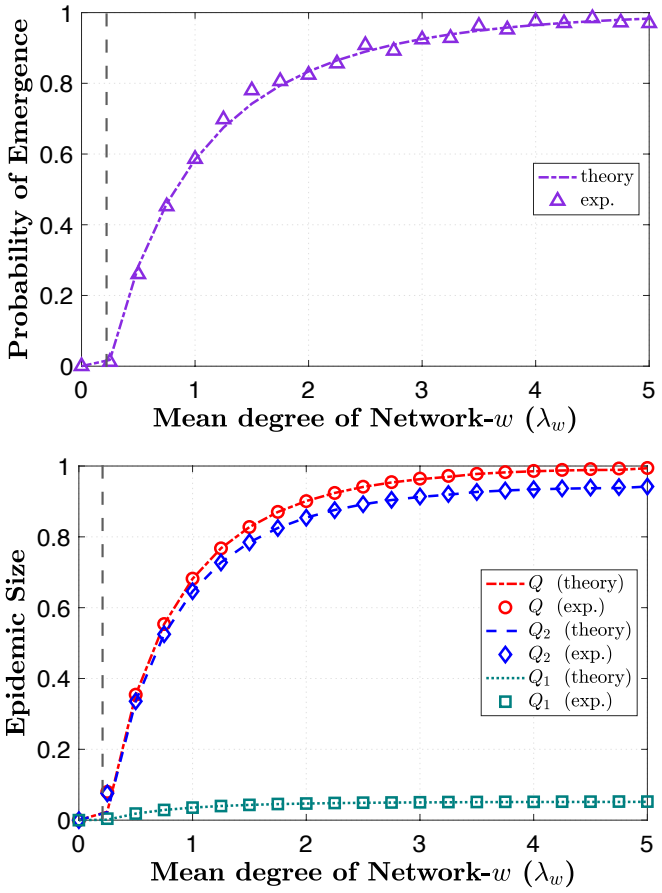

Fig. 3. Probability of emergence and the fraction of individuals infected with each strain (Q_1, Q_2) for a contact network comprising two Poisson layers with mean degrees λ_f and λ_w. We set $T_1^f = 0.6, T_2^f = 0.8, T_1^w = 0.7, T_2^w = 0.9, \mu_{11}^f = \mu_{11}^w = 0.1, \mu_{22}^f = \mu_{22}^w = 0.95$, and $n = 10000$. We set $\lambda_f = 1$ and vary λ_w in $[0, 5]$. The theoretical probability, epidemic size, and transition points are derived from Theorems 1–3, respectively, while the experimental results correspond to averaging over 500 independent experiments.

a different initialization for the transmission parameters with $T_1^f = 0.5$, $T_2^f = 0.7$, $T_1^w = 0.3$, $T_2^w = 0.4$, $\mu_{11}^f = \mu_{11}^w = 0.2$, $n = 10000$, and $\mu_{22}^f = \mu_{22}^w = 0.5$. To demonstrate the impact of increasing edge density in the contact network, we vary the mean node degree while keeping transmission and mutation parameters fixed. In Figure 4, we vary λ_f and λ_w in $[1, 3]$ and plot the probability of emergence and epidemic size averaged over 1000 independent experiments. We observe a good agreement between our analytical results in Theorems 1–3 and simulations in Figs. 3 and 4.

Discussion

Joint Impact of Layer Openings and Mutations. In this section, we discuss the interplay of layer openings and mutations on the probability of emergence of epidemic outbreaks. We consider the case where the fitness landscape consists of two strains. The process starts when the population is introduced to the first strain (strain 1) which is moderately transmissible and initially dominant in the population. In contrast, the other strain (strain 2) is highly transmissible and initially absent in the population but has the risk of emerging through mutations in strain 1. For modeling mutations that occur within hosts, we assume that the mutation probabilities depend on the type of strain but not on the type of link over which the infection was transmitted. We let $\boldsymbol{\mu}$ denote the mutation matrices in the two layers ($\boldsymbol{\mu} = \boldsymbol{\mu}^f = \boldsymbol{\mu}^w$), and let $\mu_{22} \to 1$, wherein with high probability, once the pathogen mutates to strain 2, it does not mutate back to strain 1. In particular, we consider the mutation and transmission matrices below:

$$\boldsymbol{\mu} = \begin{bmatrix} \mu_{11} & 1-\mu_{11} \\ 0 & 1 \end{bmatrix}, 0 < \mu_{11} < 1, \quad [18]$$

$$\begin{bmatrix} T_1^w & 0 \\ 0 & T_2^w \end{bmatrix} = c \begin{bmatrix} T_1^f & 0 \\ 0 & T_2^f \end{bmatrix}, c \geq 1; T_1^w < T_2^w, T_1^f < T_2^f. \quad [19]$$

The above mutation and transmission parameters in Eq. **18** correspond to the one-step irreversible mutation scheme, which is used widely (27, 69) to model scenarios where a simple change is required for the contagion to evolve to a highly transmissible variant. We first derive a result characterizing the epidemic threshold for one-step irreversible mutations.

Lemma 2. *For the one-step irreversible mutation matrix given by Eq.* ***18*** *and transmissibilities satisfying* Eq. **19**, *the epidemic threshold does not depend on* μ_{11} *or* T_1^f. *Specifically,*

$$\rho(\boldsymbol{J}) = T_2^f \times \rho\left(\begin{bmatrix} \beta_f & c\lambda_w \\ \lambda_f & c\beta_w \end{bmatrix}\right). \quad [20]$$

A proof for Lemma 2 is provided in *SI Appendix*, 2.A.

In cases where the initial strain by itself is not transmissible enough to cause an epidemic and the course of the epidemic is tied to the emergence of a highly transmissible strain, it is of interest to ascertain the probability that at least one mutation to strain 2 occurs in the chain of infections initiated by the introduction of strain 1 to a susceptible population. Note that the above quantity is different from the probabilities given by the mutation matrix Eq. **18**, which defines the probability of mutation to a different strain (within each host) after every transmission event.

Lemma 3. *For the one-step irreversible mutation matrix given by Eq.* ***18*** *and transmissibilities satisfying* Eq. **19**, *we have*

$$\mathbb{P}[\textit{at least 1 mutation to strain 2}] = 1 - g(1 - T_1^f + T_1^f \mu_{11} q^f, 1 - T_1^w + T_1^w \mu_{11} q^w), \quad [21]$$

where

$$q^f = G^f(1 - T_1^f + T_1^f \mu_{11} q^f, 1 - T_1^w + T_1^w \mu_{11} q^w), \quad [22]$$

$$q^w = G^w(1 - T_1^f + T_1^f \mu_{11} q^f, 1 - T_1^w + T_1^w \mu_{11} q^w). \quad [23]$$

Here, for $a \in \{f, w\}$, q^a corresponds to the probability of there being no mutation to strain 2 in the chain of infections emanating from a later generation infective that was infected through a type a edge (*SI Appendix*, 2.B). Using Lemma 3, we derive a lower bound on the probability of emergence highlighting the role of mutations in *SI Appendix*, 2.C.

Next, we provide a parametrization of the multilayer multistrain model to jointly characterize the transition from a single layer to a multilayer setting and a single strain to a multistrain setting. We note that under the one-step irreversible mutation

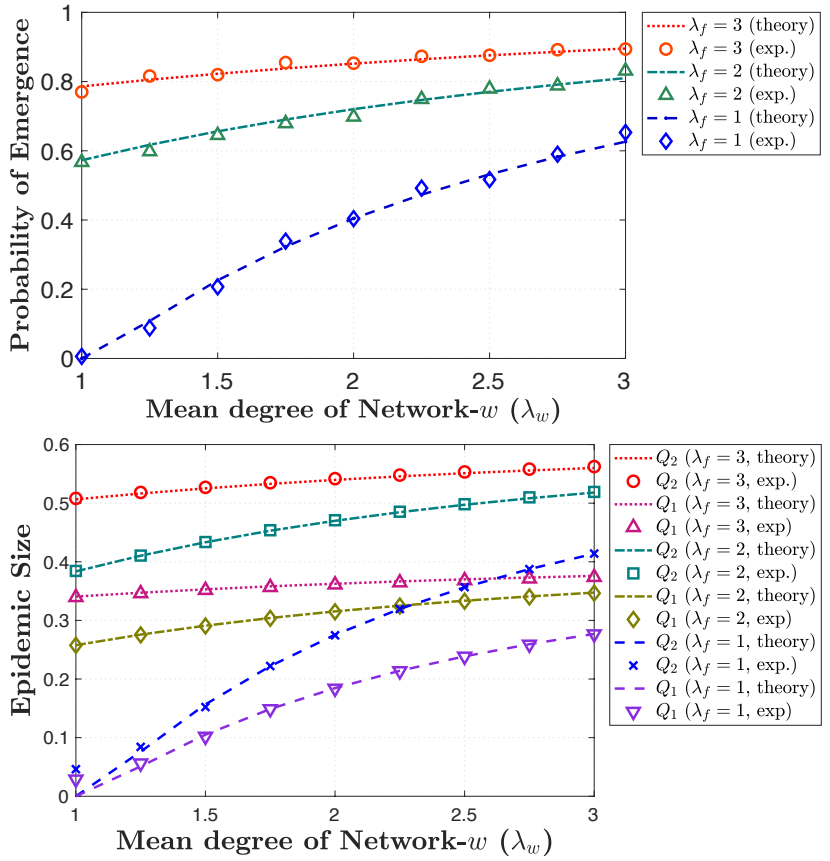

Fig. 4. Probability of emergence and the expected epidemic size for a contact network comprising two Poisson layers with mean degrees λ_f and λ_w, respectively. The fixed parameters are $T_1^f = 0.5$, $T_2^f = 0.7$, $T_1^w = 0.3$, $T_2^w = 0.4$, $\mu_{11}^f = \mu_{11}^w = 0.2$, $\mu_{22}^f = \mu_{22}^w = 0.5$, n = 10,000, and we vary λ_f and λ_w in the interval [1, 3].

matrix Eq. **18**, as μ_{11} approaches one, it corresponds to the case of the spread of contagions without mutations. Thus, the deviation of μ_{11} away from one provides a way to characterize the departure from the case where no mutations take place. Similarly, to characterize the transition from a single layer to a multilayer network, we consider the following degree distributions for the two layers:

$$d^f \sim \begin{cases} 0 \text{ w.p. } \alpha_f \\ \text{Poisson}(\nu_f) \text{ w.p. } 1-\alpha_f, \end{cases}$$
$$d^w \sim \text{Poisson}(\nu_w). \qquad [24]$$

As $\alpha_f \to 1$, no nodes participate in layer f, and the contact network $\mathbb{H}$ comprises only a single layer $\mathbb{W}$. While, when $\mu_{11} \to 1$, no mutations to strain 2 appear with high probability (whp) starting from strain 1 as described in Fig. 5.

Next, we investigate the joint impact of layer openings and mutations on the probability of emergence of an epidemic outbreak. For the domain $(\alpha_f, \mu_{11}) \in [0, 1) \times [0, 1)$ in Fig. 5, we plot the corresponding probability of emergence of an epidemic as given by Theorem 1 in Fig. 6. We set the degree distribution of the two layers as per Eq. **24** with $\nu_f = \nu_w = 1.2$. We let $c = 1, 1.5$ and plot the probability of emergence for different transmissibility values. In the light of Lemma 2, which states that the epidemic threshold is not affected by μ_{11}, it may be tempting to consider a single-strain model as being sufficient to capture the epidemic characteristics. However, in Fig. 6, we observe that adding an additional network layer can increase the risk of an epidemic by providing additional pathways for mutation. Moreover, there is a spectrum of intermediate values that the probability of emergence admits across the domain, with the single-layer or single-strain cases capturing only the limiting cases where α_f and μ_{11} respectively approach one. We observe that for regions where there is effectively just a single layer ($\alpha_f \to 1$), the probability of emergence remains relatively low despite the possible emergence of a highly contagious strain. Likewise, in cases where only a single, moderately transmissible strain

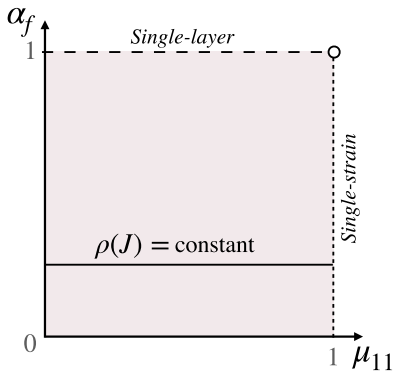

Fig. 5. A parameterization of the multilayer multistrain model as it transitions from the presence of one layer to two layers and one strain to two strains. Here, $\alpha_f \to 1$ corresponds to the case when there are no links in layer f, and the contact network $\mathbb{H}$ effectively has a single layer $\mathbb{W}$, whereas $\mu_{11} \to 1$ corresponds to the case where no mutations to a different strain occur starting from strain 1 with high probability. The horizontal lines correspond to contours with a constant epidemic threshold (Lemma 2).

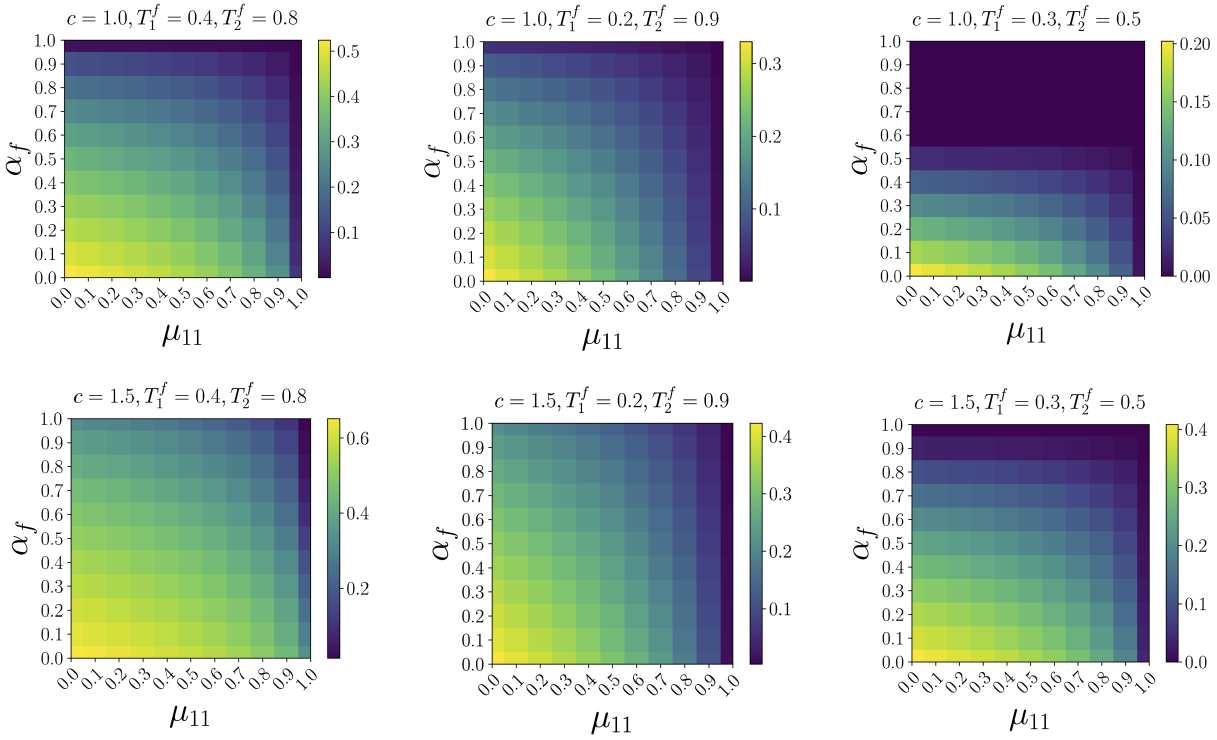

Fig. 6. For the case of one-step irreversible mutations Eq. **18**, we plot the analytical probability of emergence of an epidemic as obtained from Theorem 1. We vary $(\alpha_f, \mu_{11}) \in [0, 1) \times [0, 1)$ as characterized in Fig. 5. A smaller value of α_f and μ_{11}, respectively, correspond to a case with a greater participation in layer f and a higher probability of mutation to strain 2. We set $T_1^f = 0.4$, $T_2^f = 0.8$, $c = T_1^w/T_1^f = T_2^w/T_2^f = 1.0, 1.5$, and $\nu_f = \nu_w = 1.2$. We observe a relatively low probability of emergence when i) there is a single layer present, i.e., $\alpha_f \to 1$ (even with the highly contagious strain circulating), and ii) with a single strain circulating, i.e., $\mu_{11} \to 1$ (even when the f layer is added). However, when both layers are open and mutations occur with a positive probability, we see a higher probability of emergence.

circulates with a high probability ($\mu_{11} \to 1$), even the addition of another layer f does not lead to a high probability of emergence. In contrast, when both network layers are present, and there is a nonzero probability of mutation to strain 2, the probability of emergence is high. In Fig. 6, for the network parameters under consideration, this effect is particularly pronounced in certain transmissibility values, e.g., with $c = 1$, $T_1^f = 0.4$, $T_2^f = 0.8$, where with only a single layer open ($\alpha_f \to 1$) or a single circulating strain $\mu_{11} \to 1$, the probability of emergence remains zero. However, as layer f is opened ($\alpha_f < 1$) and there is a positive probability of mutation to strain 2 ($\mu_{11} < 1$), the probability of emergence rises to greater than 0.5 as $\mu_{11}, \alpha_f \to 0$. Likewise, when $c = 1.5$, with $T_1^f = 0.3$, $T_2^f = 0.5$, we observe that the probability jumps to over 0.4 when $\mu_{11}, \alpha_f \to 0$. In *SI Appendix*, 2.D, we demonstrate that for a more general class of network parameters, there exists a range of transmissibility values where we observe the above phenomenon under the conditions in Eqs. **18** and **19**.

The observations in Fig. 6 shed light on the impact of imposing/lifting mitigation measures concerning different contact network layers (e.g., school closures or many companies adopting work-from-home policies) on the emergence of more transmissible variants. For example, opening a new layer in the contact network may be deemed safe based on the transmissibility of the initial strain, but even a modest increase in infections caused by the new layer might increase the chances of a more transmissible strain to emerge, which in turn can make an epidemic more likely. Thus, by studying the mutations over a multilayer network, our results can help understand the comprehensive impact of layer closures/openings.

Reductions to Simpler Models. In this section, we propose and analyze approaches to reduce the multistrain multilayer (MS-ML) model into a corresponding single-strain multilayer (SS-ML) or a multistrain single-layer (MS-SL) model.

We first investigate whether, under arbitrary distributions for the network layers, we can systematically reduce the MS-ML model into an equivalent (yet simpler) MS-SL model (27) and get accurate predictions for key epidemiological quantities. In what follows, we show that when the degree distribution for the two network layers is Poisson with parameters λ_f and λ_w, respectively, the following transformation to a MS-SL model can accurately predict the probability of emergence of an epidemic (*SI Appendix*, 3.A)

$$\lambda \leftarrow \lambda_f + \lambda_w. \qquad [25]$$

$$T_1 \leftarrow \frac{\lambda_f T_1^f + \lambda_w T_1^w}{\lambda_f + \lambda_w}; \quad T_2 \leftarrow \frac{\lambda_f T_2^f + \lambda_w T_2^w}{\lambda_f + \lambda_w}. \qquad [26]$$

Next, we illustrate the potential pitfall of mapping a multilayer network to a single-layer structure using the transformations Eqs. **25–26** when the Poisson assumption no longer holds. Specifically, we study how well the reduction to a single layer allows us to predict the epidemic threshold for a multilayer network for a more general family of distributions. We first consider the case when the ratio of the transmissibilities in the two network layers is one for both strains, i.e., $\frac{T_1^w}{T_1^f} = \frac{T_2^w}{T_2^f} = 1$. In other words, the transmissibilities only depend on the type of strain and are agnostic of the type of link. Throughout, we let $\rho(.)$ denote the spectral radius of the matrix supplied as its argument.

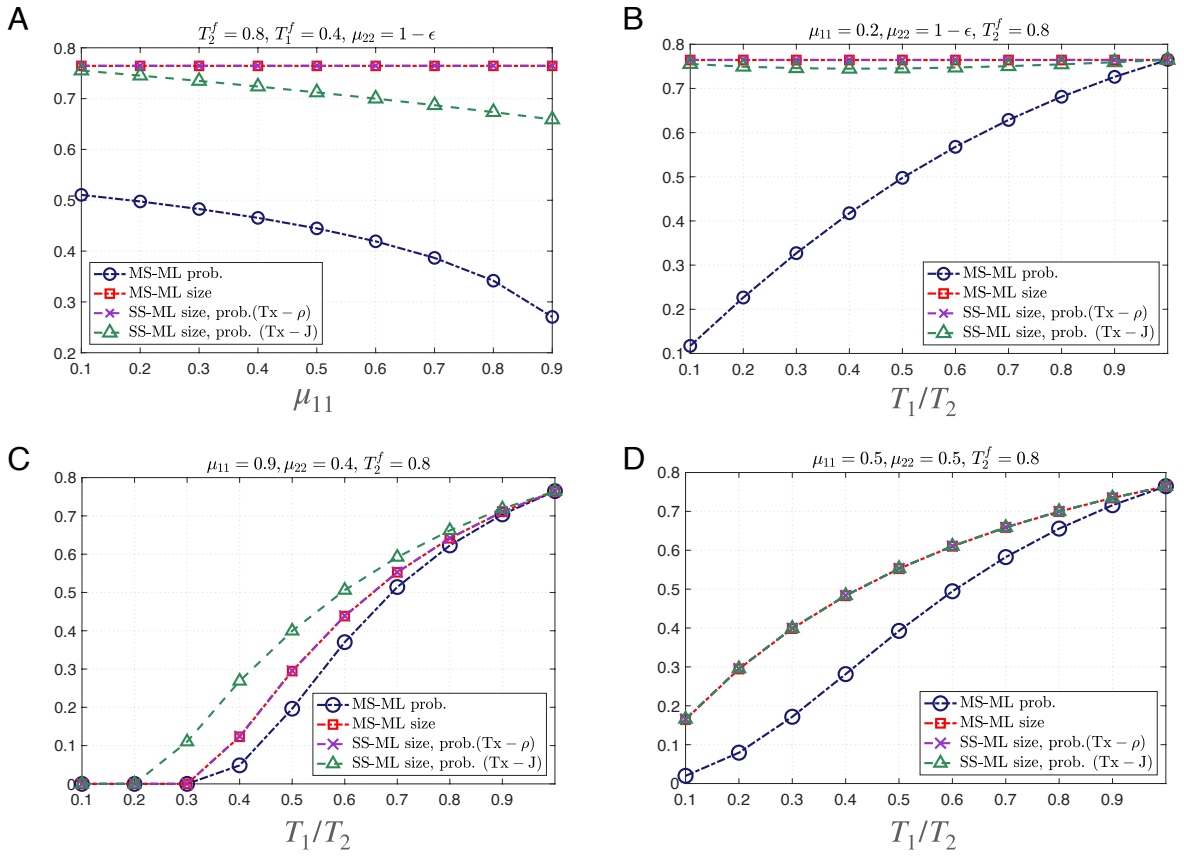

Fig. 7. A comparison of the predictions made by reduction to a single-strain (SS-ML) through mapping the spectral radius (denoted as Tx − ρ) and mapping the mean matrix for infections (denoted as Tx − J). (*A*) We set $\mu_{22} = 1 - \epsilon$ with $\epsilon = 10^{-10}$ and vary μ_{11}. Next, we set $T_2^f = 0.8$ and vary the ratio $T_1^f/T_2^f = T_1^w/T_2^w$, denoted as T_1/T_2 on the X-axis. (*B*) We set $\mu_{11} = 0.2$ and $\mu_{22} = 1 - \epsilon$. (*C*) We set $\mu_{11} = 0.9$ and $\mu_{22} = 0.4$. (*D*) We set $\mu_{11} = 0.5$ and $\mu_{22} = 0.5$. We observe that neither transformation accurately predicts the probability of emergence, and the gap in prediction is more pronounced when the difference in strain transmissibilities is higher.

Let the single-layer network obtained by taking the sum of node degrees in the two layers be denoted by $\tilde{\mathbb{H}}$. Since the layers in the multilayer network have independent degree distributions, the degree distribution for $\tilde{\mathbb{H}}$ is given by $\tilde{p} = p^f * p^w$, where $*$ denotes the convolution operator. For $a \in \{f, w\}$, recall that λ_a and β_a, respectively, denote the mean degree distribution and the mean excess degree of distribution for network layer a. Note that for network $\tilde{\mathbb{H}}$, the mean degree and mean excess degree, respectively, denoted by $\tilde{\lambda}$ and $\tilde{\beta}$ are given as

$$\tilde{\lambda} = \lambda_w + \lambda_f, \qquad [27]$$

$$\tilde{\beta} = \frac{\beta_f\lambda_f + \beta_w\lambda_w + 2\lambda_f\lambda_w}{\lambda_f + \lambda_w}. \qquad [28]$$

From Eq. **12**, it follows that for the multilayer network $\mathbb{H} = \mathbb{W} \cup \mathbb{F}$, the critical threshold for the emergence of the epidemic outbreak is

$$\rho\left(\begin{bmatrix} \beta_f & \lambda_w \\ \lambda_f & \beta_w \end{bmatrix}\right) \times \rho\left(\boldsymbol{T}^{\boldsymbol{f}}\boldsymbol{\mu}\right) > 1. \qquad [29]$$

Upon mapping the transmissibilities as per Eq. **26**, the critical threshold for the emergence of the epidemic outbreak in $\tilde{\mathbb{H}}$ (constructed using the configuration model with degree drawn from the distribution $p^f * p^w$) is given by

$$\frac{\beta_f\lambda_f + \beta_w\lambda_w + 2\lambda_f\lambda_w}{\lambda_f + \lambda_w} \times \rho\left(\boldsymbol{T}^{\boldsymbol{f}}\boldsymbol{\mu}\right) > 1. \qquad [30]$$

Comparing the above thresholds in Eqs. **29** and **30**, we see that the predicted thresholds are identical if and only if

$$\rho\left(\begin{bmatrix} \beta_f & \lambda_w \\ \lambda_f & \beta_w \end{bmatrix}\right) = \frac{\beta_f\lambda_f + \beta_w\lambda_w + 2\lambda_f\lambda_w}{\lambda_f + \lambda_w}. \qquad [31]$$

In *SI Appendix*, 3.B, we show that with $\lambda_f, \lambda_w, \beta_f, \beta_w > 0$, Eq. **31** holds if and only if

$$\beta_f - \lambda_f = \beta_w - \lambda_w. \qquad [32]$$

The condition Eq. **32** is equivalent to the dispersion indices of the constituent network layers being the same, where the dispersion index is defined as the ratio of the variance and mean of a degree distribution. For cases when the degree distribution of the constituent network layers is not from the same parametric family of distributions, depending on the magnitude of the dispersion index relative to one, the condition Eq. **32** may not hold. For instance, if the degree distribution of the two layers is respectively Poisson and Binomial, regardless of the choice of parameters of the distributions, the condition $\beta_f - \lambda_f = \beta_w - \lambda_w$ will never hold since the dispersion index of the Poisson distribution and the Binomial distribution are respectively $= 1$ and > 1. Likewise for the parameterization of the degree that accounts for nonparticipation in layer f through Eq. **24**, as long as $\alpha_f > 0$, the dispersion indices of layers f and w do not match and thus reductions to MS-SL models can yield inaccurate predictions for the epidemic threshold.

So far, we have investigated reductions to a multistrain single-layer model (MS-SL). Then, a natural question is whether we can alternatively use a reduction to a single-strain multilayer (SS-ML) model to characterize the epidemic. It is known (15, 34) that when there are correlations between infection events, the predictions made by models that assume independent transmission events can lead to incorrect predictions. For the multistrain transmission model, the infection events are conditionally independent given the type of strain carried by a node and dependent otherwise. Therefore, models that do not account for correlation in infection events, such as single-strain spreading on multilayer networks (47), can lead to inaccurate predictions for multistrain settings; see ref. 34 for a detailed discussion. We evaluate reductions to SS-ML models, assuming $T_1^w/T_1^f = T_2^w/T_2^f = c$, by considering the following two approaches. The first approach, denoted as $\mathrm{Tx}-\rho$, involves using Eq. **12** and defining the equivalent transmissibilities for the two layers as

$$\rho(\boldsymbol{T^f\mu}) \to \tilde{T}^f,\ \rho(\boldsymbol{T^w\mu}) \to \tilde{T}^w (\equiv c\rho(\boldsymbol{T^f\mu}) \to \tilde{T}^w). \quad [\mathbf{33}]$$

Through Eq. **12**, the transformation Eq. **33** ensures that the epidemic threshold predicted by the corresponding SS-ML reduction is the same as the MS-ML model. The second approach, denoted as $\mathrm{Tx}-J$, is based on transforming to a single layer by directly matching the mean matrix, i.e., we ensure that the mean number of secondary infections stemming from any given type of infected individual is the same across the models (*SI Appendix*, 4).

Next, we evaluate the above reductions to SS-ML models. Following the network distribution in Eq. **24**, we set $\alpha_f = 0.2$, $\alpha_w = 0$, $\nu_f = \nu_w = 1.2$, $T_2^f = 0.8$, and we assume $T_1^w/T_1^f = T_2^w/T_2^f = c = 1.2$. In Fig. 7*A*, we fix the transmissibility parameters and plot the predictions made by the above transformations to SS-ML models. We set $\mu_{22} = 1-\epsilon$ with $\epsilon = 10^{-10}$ and vary μ_{11} in the interval $[0, 1]$. From Lemma 2, we know that as $\mu_{22} \to 1$, $\rho(\boldsymbol{T^f\mu})$ remains constant, and thus, the prediction made by the SS-ML under the $\mathrm{Tx}-\rho$ mapping remains constant. We note that one general shortcoming of the SS-ML transformations is that they predict the same probability of emergence and epidemic size; they can at best only predict one of these metrics accurately. Moreover, they do not shed light on the fraction of individuals infected by each strain type. Substituting $T_1^f = T_2^f = \rho(\boldsymbol{T^f\mu})$ and $T_1^w = T_2^w = c\rho(\boldsymbol{T^f\mu})$ and $\boldsymbol{\mu^f} = \boldsymbol{\mu^w} = \boldsymbol{I_2}$ in Theorem 1, we get the predictions for the SS-ML model under the $\mathrm{Tx}-\rho$. We note that while the SS-ML reduction through mapping the spectral radius ($\mathrm{Tx}-\rho$) captures the size, it fails to predict the probability of emergence. This observation is consistent with the observation that reducing an MS-SL model to a bond-percolation model leads to inaccurate prediction for the probability of emergence but correctly predicts the total epidemic size (34).

In Fig. 7 *B*–*D*, we vary the ratio $T_1^f/T_2^f = T_1^w/T_2^w$, denoting it by T_1/T_2 while keeping T_2^f constant at 0.8. We observe that mapping through $\mathrm{Tx}-J$ neither accurately predicts the epidemic size nor the probability of emergence. We observe that the gap in the prediction of the probability of emergence by the SS-ML models is less pronounced when $T_1/T_2 \to 1$. Further, when $\mu_{22} \to 1$, the predictions made by mapping the spectral radius are constant in line with Lemma 2. As above, the SS-ML model under the $\mathrm{Tx}-\rho$ transformation captures the size and the epidemic threshold while failing to predict the probability of emergence accurately. We note that both the transformations (matching the epidemic threshold and the mean mutation matrix) critically relied on the decoupling Eq. **12**, which only holds when $T_1^f/T_1^w = T_2^f/T_2^w$. Our observations further highlight the importance of developing epidemiological models that account for the heterogeneity in network structure and pathogen strains.

Conclusion

This work analyzed the spreading characteristics of mutating contagions over multilayer networks. We derived the fundamental epidemiological quantities for the proposed multilayer multistrain model: the probability of emergence, the epidemic threshold, and the mean fraction of individuals infected with each strain. Our findings underscore that we should evaluate the impact of imposing/lifting mitigation measures concerning different contact network layers in relation to their effect on the emergence of new strains. We showed that transformations to existing models can inaccurately characterize the multilayer multistrain setting while also unraveling conditions under which simpler models can help make predictions.

An important future direction is to extend the network-based analysis of multistrain spreading (27) to allow for the case when the previous infection with one strain confers full immunity only with respect to that strain while leaving the individual susceptible to other strains, although possibly at a reduced level. While cross-immunity among different pathogen strains has been studied (37) in multispreading models that do not account for the contact network structure, it is of interest to research cross-immunity interference in the light of different contact patterns. Such an analysis will pave the way for evaluating the risk of the emergence of new strains that can evade immunity acquired from previous infections or vaccination in the light of different policy measures that alter the contact network.

Future work might also focus on extending the contact network model used in this paper to better capture the real-world spreading events. While the framework proposed here allows us to model networks with arbitrary degree distributions, future work can explore extending the framework to incorporate more modes of node heterogeneity, such as tunable clustering (18) and community structures (70). Further investigation of the multilayer framework can also shed light on the impact of superspreading events such as concerts and sports games. We can utilize the multilayer framework to model such events by incorporating an extra layer with a high degree of connectivity to the existing contact network. For a more realistic representation, the additional layer can be dynamic because nodes that participate in the layer may change over time, or the layer may exist only for a short period of time. The multilayer network model can also be leveraged to represent different connectivity patterns that might exist among different subgroups of individuals. More generally, we can construct a model where a base network layer includes every individual, with a certain level of connectivity among them. Overlaying this, we might have multiple layers, each representing a specific age group or a demographic to represent the additional connectivity we expect among that group. It is also of interest to investigate the impact of rare events of untraceable contacts and develop models to account for untraceable nodes and contacts in contact-tracing tools (71). Finally, in the context of social networks, a promising future application is to leverage models for multistrain spreading to combat the spread of misinformation across different social media platforms.

Data, Materials, and Software Availability. The code for the simulations in the paper is available in ref. 72, and all proofs are available in *SI Appendix*.

ACKNOWLEDGMENTS. This research was supported in part by the NSF through grants 2225513, 2026985, 1813637, CCF-2142997, CNS-2041952, and CCF-1917819; the Army Research Office through grants W911NF-22-1-0181, W911NF-20-1-0204, and W911NF-18-1-0325; an IBM academic award; a gift from Google; and Dowd Fellowship, Knight Fellowship, Lee-Stanziale Ohana Endowed Fellowship, and Cylab Presidential Fellowship from Carnegie Mellon University.

Author affiliations: [a]Department of Electrical and Computer Engineering, Carnegie Mellon University, Pittsburgh, PA 15213; [b]Department of Electrical Engineering, Princeton University, Princeton, NJ 08544; [c]Rocket Travel, Inc., Chicago, IL 60661; [d]Thomas J. Watson Research Center, IBM, Yorktown Heights, NY 10598; [e]Department of Ecology and Evolutionary Biology, Princeton University, Princeton, NJ 08544; and [f]Software and Societal Systems Department, Carnegie Mellon University, Pittsburgh, PA 15213

1. World Health Organization, Coronavirus Disease (Covid-19), 21 September 2020, Technical Documents (2020).
2. W. T. Harvey *et al*., SARS-CoV-2 variants, spike mutations and immune escape. *Nat. Rev. Microbiol.* **19**, 409–424 (2021).
3. S. Islam, T. Islam, M. R. Islam, New coronavirus variants are creating more challenges to global healthcare system: A brief report on the current knowledge. *Clin. Pathol.* **15**, 2632010X221075584 (2022).
4. J. S. Tregoning, K. E. Flight, S. L. Higham, Z. Wang, B. F. Pierce, Progress of the Covid-19 vaccine effort: Viruses, vaccines and variants versus efficacy, effectiveness and escape. *Nat. Rev. Immunol.* **21**, 626–636 (2021).
5. R. M. Burgos *et al*., The race to a Covid-19 vaccine: Opportunities and challenges in development and distribution. *Drugs Context* **10**, 1–10 (2021).
6. C. Beyrer *et al*., Human rights and fair access to Covid-19 vaccines: The International Aids Society-Lancet Commission on Health and Human Rights. *Lancet* **397**, 1524–1527 (2021).
7. L. Matrajt, T. Leung, Evaluating the effectiveness of social distancing interventions to delay or flatten the epidemic curve of coronavirus disease. *Emerg. Infect. Dis.* **26**, 1740 (2020).
8. S. Eubank *et al*., Commentary on Ferguson, et al.,"Impact of non-pharmaceutical interventions (NPIs) to reduce Covid-19 mortality and healthcare demand". *Bull. Math. Biol.* **82**, 1–7 (2020).
9. D. H. Morris, F. W. Rossine, J. B. Plotkin, S. A. Levin, Optimal, near-optimal, and robust epidemic control. *Commun. Phys.* **4**, 1–8 (2021).
10. A. Mandel, V. Veetil, The economic cost of Covid lockdowns: An out-of-equilibrium analysis. *Econ. Disasters Clim. Change* **4**, 431–451 (2020).
11. C. Arndt *et al*., Covid-19 lockdowns, income distribution, and food security: An analysis for South Africa. *Global Food Sec.* **26**, 100410 (2020).
12. F. Brauer, "Compartmental models in epidemiology" in *Mathematical Epidemiology* (Springer, 2008), pp. 19–79.
13. R. M. Anderson, R. M. May, *Infectious Diseases of Humans: Dynamics and Control* (Oxford University Press, 1992).
14. M. E. Newman, Spread of epidemic disease on networks. *Phys. Rev. E* **66**, 016128 (2002).
15. E. Kenah, J. M. Robins, Second look at the spread of epidemics on networks. *Phys. Rev. E* **76**, 036113 (2007).
16. M. Salathé *et al*., A high-resolution human contact network for infectious disease transmission. *Proc. Natl. Acad. Sci. U.S.A.* **107**, 22020–22025 (2010).
17. K. Sun *et al*., Transmission heterogeneities, kinetics, and controllability of SARS-CoV-2. *Science* **371**, eabe2424 (2021).
18. Y. Zhuang, A. Arenas, O. Yağan, Clustering determines the dynamics of complex contagions in multiplex networks. *Phys. Rev. E* **95**, 012312 (2017).
19. H. S. Monteiro *et al*., Superspreading k-cores at the center of Covid-19 pandemic persistence. *Bull. Am. Phys. Soc.* **66** (2021).
20. Q. Zeng, Y. Liu, M. Tang, J. Gong, Identifying super-spreaders in information-epidemic coevolving dynamics on multiplex networks. *Knowledge-Based Syst.* **229**, 107365 (2021).
21. M. K. So, A. M. Chu, A. Tiwari, J. N. Chan, On topological properties of Covid-19: Predicting and assessing pandemic risk with network statistics. *Sci. Rep.* **11**, 1–14 (2021).
22. L. Hébert-Dufresne, P. A. Noël, V. Marceau, A. Allard, L. J. Dubé, Propagation dynamics on networks featuring complex topologies. *Phys. Rev. E* **82**, 036115 (2010).
23. S. Thurner, P. Klimek, R. Hanel, A network-based explanation of why most Covid-19 infection curves are linear. *Proc. Natl. Acad. Sci. U.S.A.* **117**, 22684–22689 (2020).
24. J. Chen *et al*., Networked epidemiology for Covid-19. *SIAM News* **53** (2020).
25. C. Bongiorno, L. Zino, A multi-layer network model to assess school opening policies during a vaccination campaign: A case study on Covid-19 in France. *Appl. Network Sci.* **7**, 1–28 (2022).
26. A. Aleta *et al*., Modelling the impact of testing, contact tracing and household quarantine on second waves of Covid-19. *Nat. Hum. Behav.* **4**, 964–971 (2020).
27. H. Alexander, T. Day, Risk factors for the evolutionary emergence of pathogens. *J. R. Soc. Interface* **7**, 1455–1474 (2010).
28. Z. W. Ye *et al*., Zoonotic origins of human coronaviruses. *Int. J. Biol. Sci.* **16**, 1686 (2020).
29. J. Cui, F. Li, Z. L. Shi, Origin and evolution of pathogenic coronaviruses. *Nat. Rev. Microbiol.* **17**, 181–192 (2019).
30. A. Latinne *et al*., Origin and cross-species transmission of bat coronaviruses in china. *Nat. Commun.* **11**, 1–15 (2020).
31. C. R. Parrish *et al*., Cross-species virus transmission and the emergence of new epidemic diseases. *Microbiol. Mol. Biol. Rev.* **72**, 457–470 (2008).
32. R. M. Anderson, R. M. May, *Infectious Diseases of Humans* (Oxford University Press, Oxford, UK, 1991).
33. Q. H. Liu *et al*., Measurability of the epidemic reproduction number in data-driven contact networks. *Proc. Natl. Acad. Sci. U.S.A.* **115**, 12680–12685 (2018).
34. R. Eletreby, Y. Zhuang, K. M. Carley, O. Yağan, H. V. Poor, The effects of evolutionary adaptations on spreading processes in complex networks. *Proc. Natl. Acad. Sci. U.S.A.* **117**, 5664–5670 (2020).
35. M. Girvan, D. S. Callaway, M. E. Newman, S. H. Strogatz, Simple model of epidemics with pathogen mutation. *Phys. Rev. E* **65**, 031915 (2002).
36. V. Andreasen, J. Lin, S. A. Levin, The dynamics of cocirculating influenza strains conferring partial cross-immunity. *J. Math. Biol.* **35**, 825–842 (1997).
37. S. Kryazhimskiy, U. Dieckmann, S. A. Levin, J. Dushoff, On state-space reduction in multi-strain pathogen models, with an application to antigenic drift in Influenza A. *PLoS Comput. Biol.* **3**, e159 (2007).
38. B. T. Grenfell *et al*., Unifying the epidemiological and evolutionary dynamics of pathogens. *Science* **303**, 327–332 (2004).
39. E. B. O'Dea, C. O. Wilke, Contact heterogeneity and phylodynamics: How contact networks shape parasite evolutionary trees. *Interdiscip. Persp. Infect. Dis.* **2011**, 238743 (2011).
40. E. C. Holmes, B. T. Grenfell, Discovering the phylodynamics of RNA viruses. *PLoS Comput. Biol.* **5**, e1000505 (2009).
41. T. Shiino, Phylodynamic analysis of a viral infection network. *Front. Microbiol.* **3**, 278 (2012).
42. V. M. Marquioni, M. A. de Aguiar, Modeling neutral viral mutations in the spread of SARA-CoV-2 epidemics. *PLoS ONE* **16**, e0255438 (2021).
43. X. Zhang *et al*., Epidemic spreading under mutually independent intra- and inter-host pathogen evolution. *Nat. Commun.* **13**, 1–13 (2022).
44. G. U. Yule *et al*., II. A mathematical theory of evolution, based on the conclusions of Dr. J.C. Willis, F.R.S. *Phil. Trans. R. Soc. Lond. B* **213**, 21–87 (1925).
45. M. Ajelli, P. Poletti, A. Melegaro, S. Merler, The role of different social contexts in shaping influenza transmission during the 2009 pandemic. *Sci. Rep.* **4**, 1–7 (2014).
46. D. Soriano-Paños, L. Lotero, A. Arenas, J. Gómez-Gardeñes, Spreading processes in multiplex metapopulations containing different mobility networks. *Phys. Rev. X* **8**, 031039 (2018).
47. O. Yağan, D. Qian, J. Zhang, D. Cochran, Conjoining speeds up information diffusion in overlaying social-physical networks. *IEEE J. Selec. Areas Commun.* **31**, 1038–1048 (2013).
48. A. Hackett, D. Cellai, S. Gómez, A. Arenas, J. P. Gleeson, Bond percolation on multiplex networks. *Phys. Rev. X* **6**, 021002 (2016).
49. G. Bianconi, Epidemic spreading and bond percolation on multilayer networks. *J. Stat. Mech.: Theory Exp.* **2017**, 034001 (2017).
50. Y. Zhuang, O. Yağan, Information propagation in clustered multilayer networks. *IEEE Trans. Network Sci. Eng.* **3**, 211–224 (2016).
51. P. Mann, V. A. Smith, J. B. O. Mitchell, S. Dobson, Random graphs with arbitrary clustering and their applications. *Phys. Rev. E* **103**, 012309 (2021).
52. F. D. Sahneh, C. Scoglio, P. Van Mieghem, Generalized epidemic mean-field model for spreading processes over multilayer complex networks. *IEEE/ACM Trans. Networking* **21**, 1609–1620 (2013).
53. V. Marceau, P. A. Noël, L. Hébert-Dufresne, A. Allard, L. J. Dubé, Modeling the dynamical interaction between epidemics on overlay networks. *Phys. Rev. E* **84**, 026105 (2011).
54. F. Radicchi, Percolation in real interdependent networks. *Nat. Phys.* **11**, 597 (2015).
55. N. Azimi-Tafreshi, Cooperative epidemics on multiplex networks. *Phys. Rev. E* **93**, 042303 (2016).
56. M. De Domenico, C. Granell, M. A. Porter, A. Arenas, The physics of spreading processes in multilayer networks. *Nat. Phys.* **12**, 901–906 (2016).
57. M. De Domenico *et al*., Mathematical formulation of multilayer networks. *Phys. Rev. X* **3**, 041022 (2013).
58. R. Dawkins, *The Selfish Gene* (Oxford University Press, 2016).
59. L. A. Adamic, T. M. Lento, E. Adar, P. C. Ng, "Information evolution in social networks" in *ACM WSDM* (2016), pp. 473–482.
60. B. Bollobás, *Random Graphs, Cambridge Studies in Advanced Mathematics* (Cambridge University Press, Cambridge, UK, 2001).
61. M. Molloy, B. Reed, A critical point for random graphs with a given degree sequence. *Random Struc. Algorithms* **6**, 161–179 (1995).
62. P. Haccou, P. Haccou, P. Jagers, V. A. Vatutin, V. A. Vatutin, *Branching Processes: Variation, Growth, and Extinction of Populations* (Cambridge University Press, 2005), No. 5.
63. C. J. Mode , *Multitype Branching Processes: Theory and Applications* (American Elsevier Pub. Co., 1971), vol. **34**.
64. M. E. Newman, S. H. Strogatz, D. J. Watts, Random graphs with arbitrary degree distributions and their applications. *Phys. Rev. E* **64**, 026118 (2001).
65. L. Zino, M. Cao, Analysis, prediction, and control of epidemics: A survey from scalar to dynamic network models. *IEEE Circ. Syst. Mag.* **21**, 4–23 (2021).
66. J. P. Sethna *et al*., Hysteresis and hierarchies: Dynamics of disorder-driven first-order phase transformations. *Phys. Rev. Lett.* **70**, 3347–3350 (1993).
67. B. Söderberg, Properties of random graphs with hidden color. *Phys. Rev. E* **68**, 026107 (2003).
68. A. Clauset, C. R. Shalizi, M. E. Newman, Power-law distributions in empirical data. *SIAM Rev.* **51**, 661–703 (2009).
69. R. Antia, R. R. Regoes, J. C. Koella, C. T. Bergstrom, The role of evolution in the emergence of infectious diseases. *Nature* **426**, 658 (2003).
70. R. van der Hofstad, J. Komjáthy, V. Vadon, Phase transition in random intersection graphs with communities. *Random Struct. Algorithms* **60**, 406–461 (2022).
71. A. C. Rusu, R. Emonet, K. Farrahi, Modelling digital and manual contact tracing for Covid-19. Are low uptakes and missed contacts deal-breakers? *PLoS ONE* **16**, e0259969 (2021).
72. M. Sood *et al*., Simulations from the paper 'Spreading Processes with Mutations over Multi-layer networks'. *GitHub Repository* (2023). https://github.com/mansi-sood/multilayer-multistrain-spreading-processes.